Numerical investigation on the dynamic response characteristics of a thermoelectric generator module under transient temperature excitations

Ding Luo[a], Yuying Yan[b], Ruochen Wang[a,*], Weiqi Zhou[a]

[a] School of Automotive and Traffic Engineering, Jiangsu University, Zhenjiang, 212013, China

[b] Fluids and Thermal Engineering Research Group, Faculty of Engineering, University of Nottingham, UK

Abstract: In this work, a three-dimensional transient numerical model of a thermoelectric generator module considering the temperature-dependent properties and the topological connection of load resistance is proposed to study its dynamic response characteristics. The dynamic output power and conversion efficiency of the thermoelectric generator module under steady and different transient temperature excitations are compared and studied. A time delay exists in the output response of the thermoelectric generator module, and the time delay increases when the temperature rate increases. When the heat source temperature changes rapidly, the corresponding output power, conversion efficiency, and other thermal responses will show a more stable change trend. Moreover, the dynamic response characteristic of the output power is synchronous with that of the conversion efficiency. The periodic temperature excitation may amplify the output power, where the average output power of the sine and triangle waves are 4.93% and 2.82% respectively higher than the steady-state output power. However, the average conversion efficiency of both is almost identical to the steady-state conversion efficiency. The proposed model contributes to predicting the dynamic performance of thermoelectric generators, and can be further extended to the whole thermoelectric generator system.

Keywords: Thermoelectric generator; Time-dependent; Numerical model; Transient; Dynamic performance

Nomenclature

Symbols

c	specific heat, $J \cdot kg^{-1} \cdot K^{-1}$
$\vec{E}$	electric field density vector, $V \cdot m^{-2}$
h	convective heat transfer coefficient, $W \cdot m^{-2} \cdot K^{-1}$
I	output current, A
$\vec{J}$	current density vector, $A \cdot m^{-2}$
P	output power, W
Q	heat, W
R	electric resistance, Ω
T	temperature, K
t	time, s
U	voltage, V

Greek symbols

λ	thermal conductivity, $W \cdot m^{-1} \cdot K^{-1}$
α	Seebeck coefficient, $\mu V \cdot K^{-1}$
σ^{-1}	electrical resistivity, $10^{-5} \Omega \cdot m$
ρ	density, $kg \cdot m^{-3}$
ϕ	electric potential, V
η	conversion efficiency

Subscripts

ce	ceramic plates
co	copper electrodes
ext	external environment
h	hot side
L	load resistance
n	n-type thermoelectric elements
p	p-type thermoelectric elements
te	thermoelectric elements

1. Introduction

Given the excessive use of fossil energy, CO_2 emissions and energy shortage have become global problems. Researchers have been committed to exploring and developing alternative green energy technologies to reduce emissions and fossil fuel usage. As one of the alternative energy technologies, thermoelectric generator (TEG) can directly convert heat energy into electricity, which has attracted great interest from researchers in recent years. Compared with the traditional power generation technology, TEG has unparalleled merits, such as, no mechanical moving components, noiseless operation, flexible layout, no emissions, long service life, and so on [1, 2]. Generally, a TEG module, comprised of an array of thermoelectric units, was used as the core of power generation and sandwiched between the heat and the cooling sources. Driven by the large temperature difference, the TEG module will generate Seebeck voltage. Through an energy recovery circuit, the generated electric energy can be stored in the battery, and can also supply power for other electronic equipment.

Currently, primary applications of TEG technology have been witnessed in the fields of power supply of spacecrafts [3], waste heat recovery [4, 5], power supply of wearable devices [6], and power generation of cook stoves [7]. Taking the radioactive decay energy of $^{238}PuO_2$ as the heat source, Liu et al. [8] proposed a miniaturised radioisotope TEG on the basis of concentric filament architecture; The structure was optimised by numerical simulations, and the maximum power output of 423.50 μW was obtained at the heat source temperature of 398.15 K. Wang et al. [9] fabricated a TEG system with 240 TEG modules to recover the waste heat from automobile exhaust gases; The authors also proposed

a theoretical prediction method to evaluate the performance of the TEG system, and their research results indicated that the net power of 133.46 W was reached when the engine power and the vehicle speed were 47 kW and 125 km/h, respectively. With a layer of thermoelectric units attached to the skin, human body heat can also be used to generate electricity. Nozariasbmarz et al. [10] constructed a TEG based body heat harvesting system, and established a quasi-3D analytical model to optimize the material and device parameters; Under the condition of air forced convection cooling, the developed TEG can deliver approximately 156.5 $\mu W/cm^2$ energy density. In off-grid areas and emergencies, stove-powered TEG was an alternative method to obtain electricity. Montecucco et al. [11] presented a TEG combined heat and power system for a common solid-fuel stove, and an average power of 27 W was produced during a 2-h long experiment.

The output power and conversion efficiency are two typical parameters to characterise the TEG performance, which not only depend on the performance of thermoelectric materials but also the working conditions. Under given thermoelectric material properties and working conditions, the TEG output power and conversion efficiency can be estimated by some theoretical models, including analytical [12] and numerical models [13, 14]. The analytical model is based on the conservation of heat transfer, and the TEG output power is regarded as the difference between the heat absorption at the hot end and the heat dissipation at the cold end. Furthermore, the TEG conversion efficiency is equal to the output power divided by the heat absorption. Different from the analytical model, the numerical model is based on the partial differential equations and solved by the finite element method to obtain the physical field distribution characteristics of TEG. According to the numerical results, output power and conversion efficiency of TEG can be estimated. By comparing the analytical model with the numerical model [15, 16], the results showed that the numerical model can predict the TEG performance more reasonably and accurately than the analytical model. Therefore, more and more researchers prefer to use numerical models to optimise and predict the performance of TEG devices. Combined with the modelling of fluid flow, a comprehensive fluid-thermal-electric multiphysics numerical model [17, 18] has been established to evaluate the performance of TEG systems for fluid waste heat recovery. Several works have been carried out to develop more complete theoretical models of the TEG system in different application scenarios [19, 20].

Most of the existing TEG or TEG system models only focused on the steady-state performance evaluation [21, 22], and a few studies conducted the transient performance analysis [23, 24]. In practical applications, the temperature of heat source applied into the hot side of TEG was time-dependent, for example, in the field of automobile exhaust waste heat recovery, the exhaust

temperature varied with vehicle speed; for stove-powered TEG systems, the heat flux provided by flame was not static. In addition, when the TEG was in the start-up or shutdown stages, the output power and conversion efficiency of TEG will show the dynamic response characteristics. Consequently, the theoretical model for predicting the TEG performance should be extended from a steady to a transient state.

By integrating the heat transfer conservation equation of fluid flow into the analytical model, Lan et al. [24] established a dynamic model to evaluate the output performance of the automotive TEG system, and the output power in a dynamic driving cycle was predicted. Regarding thermal resistance as electric resistance and heat capacity as electric capacity, several one-dimensional equivalent circuit models [25, 26] were established to study the dynamic response characteristics of TEG. However, the analytical and analogy models may predict unrealistic results, and a transient numerical model must be built to predict the dynamic performance of TEG. For thermoelectric cooler (TEC) that converts electricity into heat energy, researchers [27, 28] have proposed a complete 3D transient numerical model to analyse the dynamic cooling performance of TEC. Although TEG and TEC follow the same governing equations, the boundary conditions are quite different. The transient numerical simulation of TEC is achieved by loading a transient current input, whereas the transient numerical simulation of TEG needs a dynamic heat flux input, and TEG is usually connected with the load resistance to form a complete circuit. Yan and Malen [29] proposed a one-dimensional transient numerical model of TEG, and the model was solved by a central difference approximation and explicit time marching method; The authors found that the conversion efficiency of TEG can be amplified by periodic heating. Meng et al. [30] further proposed a 3D transient numerical model to study the dynamic response characteristics of TEG under the transient inputs of hot side temperature, cold side temperature, and load current; Under the assumption of constant material properties, the response hysteresis of output power was found. Considering the temperature-dependent thermoelectric material properties, Jia et al. [31] developed a 2D transient numerical model to investigate the dynamic behaviour of a linear-shaped TEG; The results indicated that in the heating process, the output power and heat absorption will present obvious time delay, and in the cooling process, an internal heat source will be generated in the TEG. However, the transient numerical model was simplified into a 2D model in their study. In Refs. [29-31], the load resistance was absent and replaced by the input current. In practice, the electric current of TEG was generated by the temperature difference, and no input current was required. The numerical model considering the topological connection of load resistance is closer to the practical situation. Furthermore, these studies on transient numerical modelling of TEG are all based on a single

TEG unit, rather than the TEG module that was used as the basic power generation unit in actual applications. The steady-state numerical model has been extended from a TEG unit to a TEG module by numerous studies [13, 32], but there has been no investigation on the transient behaviour of TEG module. Thus, a more complete transient numerical model must be established to further analyse the dynamic response characteristics of the TEG module.

Taking a TEG module as the research object, this paper aims to develop a 3D transient numerical model of TEG considering the temperature-dependent properties and the topological connection of load resistance. The model is used to study the transient responses of output power and conversion efficiency of the TEG module under transient hot side temperature excitations. Here, six kinds of hot side temperature excitations, including step increase, step decrease, linear increase, linear decrease, sine wave, and triangular wave, are selected to conduct the dynamic performance analysis of the TEG module. The relative findings provide a new perspective for the dynamic response characteristics of TEG under practical dynamic heat source inputs. The model presented in this work can be further extended into the transient numerical model of the whole TEG system.

2. Three-dimensional transient numerical model of the thermoelectric generator

2.1 Geometry of the thermoelectric generator module

As aforementioned, in most TEG systems, the hot side working temperature of thermoelectric generator (TEG) modules provided by the heat source is time-dependent. The steady-state numerical model, which has been proved to be more reasonable than analytical models, can not be used to predict the dynamic response characteristics of TEG modules under transient heat source inputs. Therefore, a 3D transient numerical model is proposed to study the dynamic response characteristics of a given TEG module under different transient temperature excitations. The heat-electric multiphysics coupling effect, the temperature dependence of thermoelectric materials, and the topological connection of load resistance are considered in this model. As one of the most widely used thermoelectric materials, a Bi_2Te_3-based commercial TEG module was selected to conduct the dynamic performance analysis, as shown in Fig. 1. The p-type TEG elements (coloured in red) and n-type TEG elements (coloured in blue) are connected in series through copper electrodes (coloured in yellow). The dimensions of p-type elements, n-type elements, and copper electrodes are 1.4×1.4×1.0 mm^3, 1.4×1.4×1.0 mm^3, and 3.8×1.4×1.0 mm^3, respectively. Typically, a TEG module was placed between a hot side heat exchanger and a cold side heat exchanger. To withstand the mechanical stress between heat exchangers

and avoid the electric contact with them, thermoelectric elements and copper electrodes were clamped between two ceramic plates. There were 128 pairs of p- and n-type TEG elements, 256 copper electrodes, and two ceramic plates. Moreover, a load resistance (coloured in dark orange) with a size of 0.5×0.5×35.5 mm^3 was connected to the two terminals of the TEG module to form a complete electric circuit. During the numerical simulation, the load resistance response characteristics of the TEG module were studied by changing the electric resistivity of load resistance in a certain range. The datasheet regarding the material properties of the TEG module can be found in Table 1.

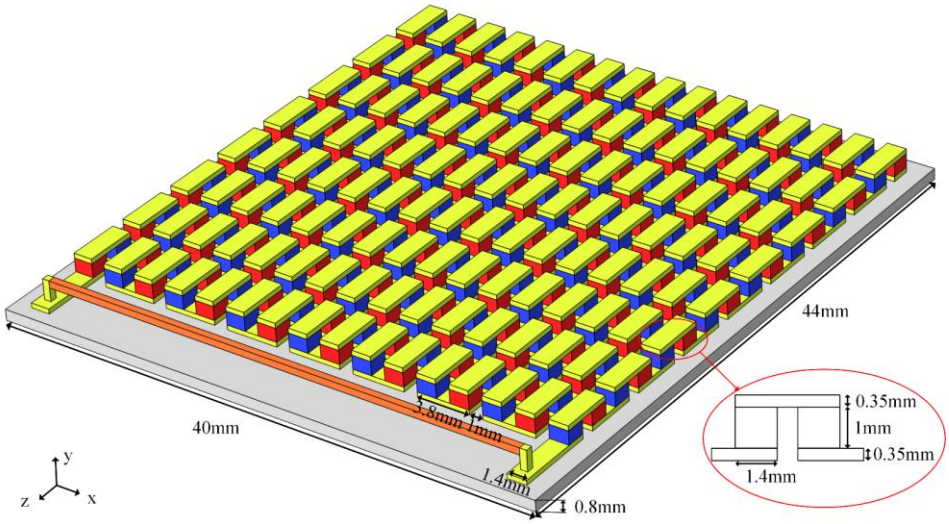

Fig. 1. Geometry of the thermoelectric generator module.

Table 1. Material properties of the thermoelectric generator module.

	n-type elements	p-type elements	copper electrodes	ceramic plates	load resistance
Thermal conductivity ($W \cdot m^{-1} \cdot K^{-1}$)	$\lambda_n(T) = -3.0595\times10^{-9}T^4 + 4.5678\times10^{-6}T^3 - 2.5162\times10^{-3}T^2 + 0.6107T - 53.9863$	$\lambda_p(T) = \lambda_n(T)$	165.64	22	400
Seebeck coefficient ($\mu V \cdot K^{-1}$)	$\alpha_n(T) = 1.8027\times10^{-7}T^4 - 3.2363\times10^{-4}T^3 + 0.2154T^2 - 62.9744T + 6616.5678$	$\alpha_p(T) = -\alpha_n(T)$	NA	NA	NA
Electric resistivity ($10^{-5}\Omega \cdot m$)	$\sigma_n^{-1}(T) = -3.088\times10^{-9}T^4 + 4.5653\times10^{-6}T^3 - 2.5854\times10^{-3}T^2 + 0.6558T - 60.588$	$\sigma_p^{-1}(T) = \sigma_n^{-1}(T)$	1.75×10^{-3}	NA	3.52~70.4
Specific heat capacity ($J \cdot kg^{-1} \cdot K^{-1}$)	188	188	381	850	381
Density ($kg \cdot m^{-3}$)	6600	6600	8978	3600	8978

2.2 Governing equations of the transient numerical model

Compared with the steady-state numerical model of thermoelectric generators, the term related to the transient change of internal energy is included in the governing equations of the transient numerical model. The transient energy conservations for p-type and n-type thermoelectric elements are expressed as:

$$(\rho c)_{\mathrm{p}} \frac{\partial T}{\partial t} = \nabla \cdot \left(\lambda_{\mathrm{p}}(T) \nabla T\right) + \sigma_{\mathrm{p}}^{-1}(T) \vec{J}^2 - \nabla \alpha_{\mathrm{p}}(T) \vec{J} T_{\mathrm{p}} \quad (1)$$

$$(\rho c)_{\mathrm{n}} \frac{\partial T}{\partial t} = \nabla \cdot \left(\lambda_{\mathrm{n}}(T) \nabla T\right) + \sigma_{\mathrm{n}}^{-1}(T) \vec{J}^2 - \nabla \alpha_{\mathrm{n}}(T) \vec{J} T_{\mathrm{n}} \quad (2)$$

where ρ, c, $\lambda(T)$, $\sigma^{-1}(T)$, and $\alpha(T)$ are the density, specific heat capacity, thermal conductivity, electric resistivity, and Seebeck coefficient of thermoelectric materials, respectively. T is the absolute temperature, t is the time, and $\vec{J}$ is the current density vector. Subscripts p and n represent p- and n-type thermoelectric elements, respectively. The first term on the left side of Eqs. (1)-(2) denotes the transient change of internal energy. On the right side of Eqs. (1)-(2), the first term denotes the Fourier thermal conduction, the second term represents the Joule heat, and the last term is the Thomson heat along thermoelectric elements or the Peltier heat on the junctions.

Given the absence of the Seebeck coefficient, the energy conservation equations of copper electrodes and load resistance are defined as:

$$(\rho c)_{\mathrm{co}} \frac{\partial T}{\partial t} = \nabla \cdot \left(\lambda_{\mathrm{co}} \nabla T\right) + \sigma_{\mathrm{co}}^{-1} \vec{J}^2 \quad (3)$$

$$(\rho c)_{\mathrm{L}} \frac{\partial T}{\partial t} = \nabla \cdot \left(\lambda_{\mathrm{L}} \nabla T\right) + \sigma_{\mathrm{L}}^{-1} \vec{J}^2 \quad (4)$$

where, subscripts co and L represent copper electrodes and load resistance, respectively.

For ceramic plates, the terms related to the electrical field are absent in the energy conservation equation, which is

$$(\rho c)_{\mathrm{ce}} \frac{\partial T}{\partial t} = \nabla \cdot \left(\lambda_{\mathrm{ce}} \nabla T\right) \quad (5)$$

where, subscript ce represents ceramic plates.

The electric current density vector in Eqs. (1)-(4) is equal to the electric field density vector multiplied by the electric conductivity of the material, which is

$$\vec{J} = \sigma \vec{E} \quad (6)$$

with

$$\vec{E} = -\nabla \phi + \alpha_{\mathrm{p,\,n}}(T) \nabla T \quad (7)$$

where, the first and second terms on the right side of Eq. (7) represent electric potential and Seebeck motive force, respectively.

In addition, the electric current through thermoelectric elements, copper electrodes, and load resistance is continuous, which can be expressed as:

$$\nabla \cdot \vec{J} = 0 \tag{8}$$

2.3 Boundary conditions of the transient numerical model

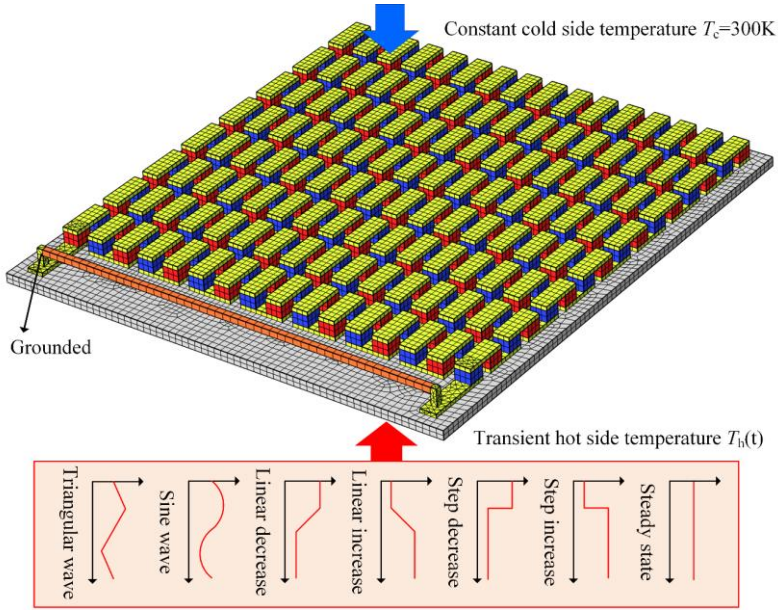

Fig. 2. Finite element model and boundary conditions of the thermoelectric generator module.

In this work, the finite element method was used to solve the above governing equations, and the finite element model of the TEG module was established by using COMSOL Multiphysics commercial software, as shown in Fig. 2. In the COMSOL platform, appropriate boundary conditions must be set to conduct the transient numerical simulations, including transient temperature boundary conditions and electric field boundary conditions. To study the dynamic response characteristics of the TEG module, seven kinds of heat source input temperature were applied on the hot side surface of the TEG module, including steady-state, step increase, step decrease, linear increase, linear decrease, sine wave, and triangular wave temperature excitations. In the steady-state, the temperature of the heat source is fixed at 450 K, whereas in the other six transient states, the temperature fluctuates between 400 K and 500 K. Fig. 3 shows the details of six transient temperature excitations. Each transient simulation starts at t = 0 s and ends at t = 8 s. The effects of different heating and cooling rates on the performance of the TEG module were studied by using the transient temperature inputs of step increase, step decrease, linear increase, and linear decrease. The effects of periodic temperature excitations on the performance of the TEG module were studied by using sine wave and triangular wave inputs.

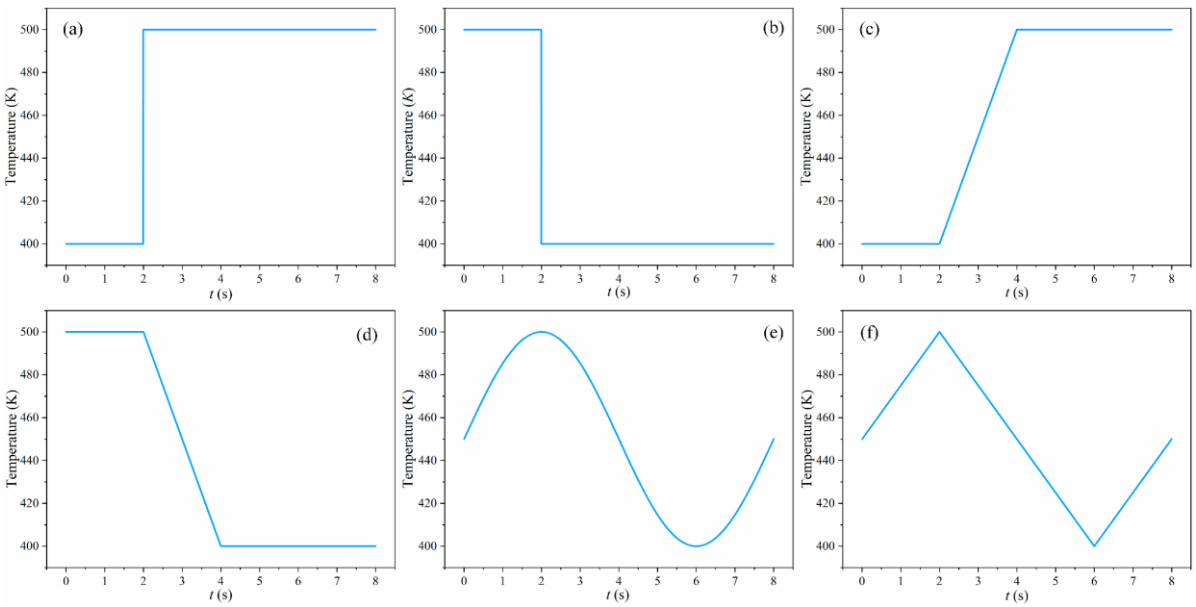

Fig. 3. Transient heat source temperature excitations as the temperature boundary conditions. (a) Step increase, (b) Step decrease, (c) Linear increase, (d) Linear decrease, (e) Sine wave, (f) Triangular wave.

In the numerical simulation, only the temperature of the heat source is transient, and other boundary conditions are all steady-state. For the cold side temperature boundary condition, a constant temperature of 300 K is applied on the cold side surface of the TEG module. The initial temperature of the TEG module is 293.15 K. In addition, the natural convection heat transfer boundary is defined on the surfaces exposed to the external environment, which is

$$-\lambda \frac{\partial T}{\partial n} = h_{\text{ext}} \left(T - T_{\text{ext}} \right) \tag{9}$$

where, T_{ext} = 293.15 K is the external temperature, and h_{ext} = 10 W·m^{-2}·K^{-1} is the external convective heat transfer coefficient.

For the voltage boundary condition of the electric field, one of the contact surfaces between load resistance and the TEG module terminal is set to be grounded. Moreover, the initial voltage of the TEG module is set as 0 V.

Combined with the governing equations and boundary conditions, the numerical results of the TEG module can be obtained by the finite element simulation. According to the numerical results, the output power P and conversion efficiency η of the TEG module are defined as:

$$P = \frac{U_{\text{L}}}{R_{\text{L}}} \tag{10}$$

$$\eta = \frac{P}{Q_{\text{h}}} \tag{11}$$

where U_L and Q_h are the output voltage and heat absorption, respectively.

3. Model validation

3.1 Grid independence examination

As shown in Fig. 2, the grid system of the TEG module comprises a large number of hexahedral meshes and a small number of tetrahedral meshes. All meshes were generated through a sweep method to ensure the high enough mesh quality. The grid independence examination was carried out in this section to select an appropriate grid size for numerical simulation. Here, the steady-state output performance of the TEG module with different mesh sizes was obtained, as listed in Table 2. The load resistance was set to be equal to 4 Ω. The error of output power increases when the mesh size increases. In theory, the numerical simulation error caused by the grid system can be reduced or even eliminated by using a sufficiently small mesh size. However, the simulation time increases when the mesh size decreases. Therefore, the mesh size of 0.6 mm was selected for the following numerical simulations to balance simulation time and model accuracy.

Table 2. Steady-state output performance of the thermoelectric generator module with different grid parameters

Mesh size (mm)	Mesh number	Output voltage (V)	Output power (W)	Error of output power
0.9	13987	3.7213	3.4620	0.25%
0.8	14445	3.7210	3.4615	0.23%
0.7	25014	3.7181	3.4561	0.08%
0.6	41023	3.7167	3.4535	0
0.5	42851	3.7167	3.4535	0

3.2 Steady-state experimental validation

The experimental and numerical results of Ref. [13] were adopted to verify the accuracy of the presented model at steady-state working conditions. In their study, the numerical results were obtained by using ANSYS 18.0/Thermal-electric, which only provides a steady-state solution. Given the limitation of the heater, the heat source input temperature can not change in a specific changing trend as the temperature excitations in Fig. 3. Consequently, the experimental verification in this work was only based on the steady-state experimental results. Moreover, the numerical results of ANSYS and COMSOL were compared to analyse the difference between the two finite element solvers. Fig. 4 shows the comparison of output voltage and output power under steady-state boundary conditions of T_h = 450 K and T_c = 320.2 K. Data show that the maximum deviation of output power between numerical results (2.25 W) of the present model and experimental results (2.28 W) is 1.56% at R_L = 9.5 Ω, and the average error of output power between COMSOL and ANSYS is 0.3%. The small

deviation shows that the proposed model can accurately predict the output performance of the TEG module. In the ANSYS platform, the Fourier heat conduction between load resistance and copper electrodes is omitted, which causes the tiny difference between ANSYS and COMSOL. In future work, the experimental apparatus will be improved, and the transient-state experiments will be conducted to verify the transient output performances.

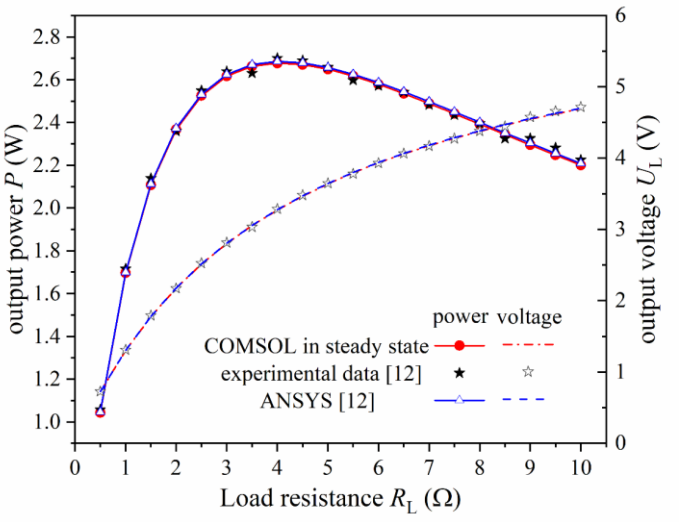

Fig. 4. Experimental validation in steady-state working conditions.

3.3 Effect of time step on the output performance of the thermoelectric generator module

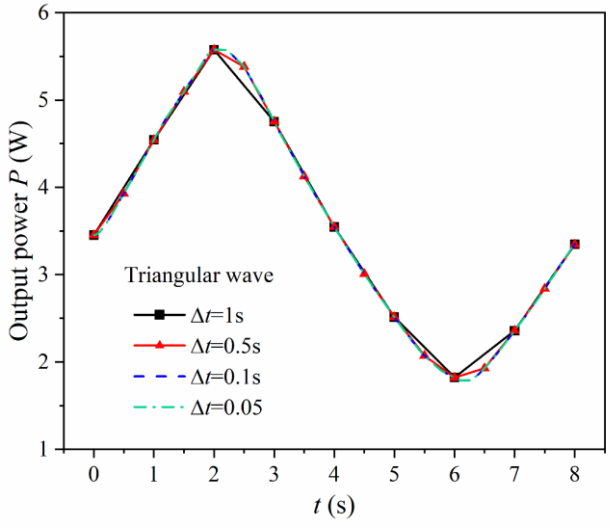

Fig. 5. Output power of the TEG module in different time steps. (e.g. triangular wave temperature excitation)

In the transient numerical simulation, not only the grid system but also the time step significantly influences the output performance of the TEG module. A large time step cause the discontinuity of simulation and result in numerical result errors, whereas a small time step will entail a long simulation

period. For this reason, taking the transient temperature excitation of the triangular wave as an example, the influence of different time steps on the output power of the TEG module is studied, as shown in Fig. 5. The results show that when the time step decreases, the change of output power tends to be gentle. When $\Delta t \leq 0.1$ s, the output power remains unchanged. Therefore, the time step of 0.1 s is used to analyse the dynamic response characteristics of the TEG module under transient temperature excitations.

4. Comparison of different transient thermal-electric numerical models

As mentioned above, 3D [30] and 2D [31] transient thermal-electric numerical models of the TEG unit have been developed in previous studies, however, the load resistance was ignored in the 3D model and replaced by the current input. The difference of this study is that the proposed 3D transient thermal-electric numerical model considers impedance matching and temperature dependence, and extends from TEG unit to TEG module. To provide a clear understanding of different transient thermal-electric numerical models, this section makes a comprehensive comparison, including a 3D transient model with impedance matching boundary, a 3D transient model with current input boundary, a 2D transient model with impedance matching boundary, and a 2D transient model with current input boundary.

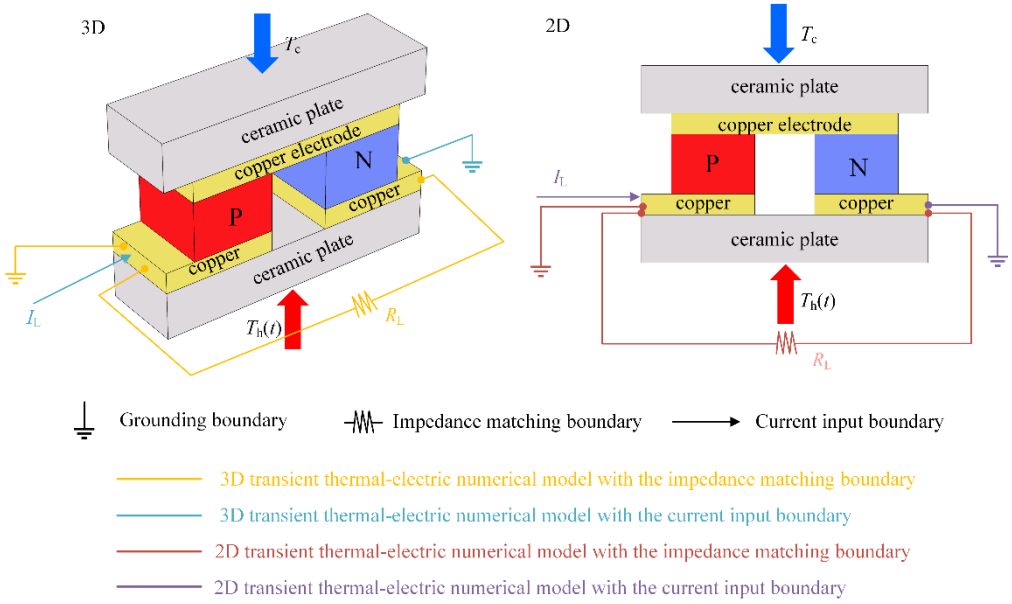

Fig. 6. Diagram of the TEG unit and the boundary conditions of different transient models.

Taking a TEG unit as the research object, its output performance predicted by different transient models is compared. Fig. 6 shows the schematic diagram of the TEG unit and the boundary conditions

of different transient models. Here, the dimensions and material parameters of the TEG unit are consistent with those of the TEG module mentioned in Section 2.1. Compared with the transient model using impedance matching boundary, the transient model using current input boundary does not need a load resistance circuit, and the circuit of the TEG unit is formed by a current input. Moreover, a transient heat source input temperature $T_h(t)$ and a steady cold side temperature T_c = 300 K were applied to the hot and cold sides of the TEG unit respectively.

Similarly, steady-state numerical simulations were carried out in advance to determine the optimal load resistance and the optimal current input. There is no difference in the optimal working points between 3D and 2D models. Therefore, the 3D model with impedance matching boundary and the 3D model with current input boundary are used to estimate the optimal load resistance and the optimal current input respectively. Fig. 7 shows the steady-state output performance of the TEG unit predicted by two 3D models at a steady heat source temperature of T_h = 450 K. According to Fig. 7(a) and Fig. 7(b), the output power of the TEG unit reaches the maximum value when R_L = 0.31 Ω and I_L = 0.92 A, respectively. As can be seen from Fig. 7(b), the steady-state output performance predicted by the model using impedance matching boundary is the same as that predicted by the model using current input boundary. However, when the input current is oversized, the output performance becomes negative, because the directional movement of carriers in thermoelectric materials is completely driven by the input current instead of the temperature difference. The thermal-electric numerical model with current input boundary can be used to predict the steady-state output performance of TEG devices in a reasonable current input range.

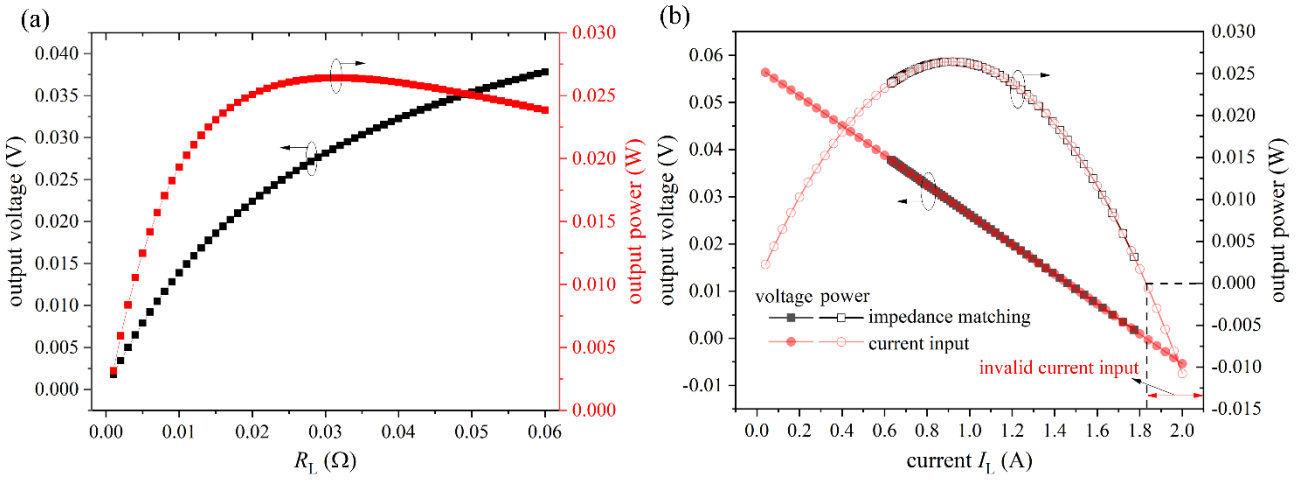

Fig. 7. Steady-state output performance of the TEG unit predicted by two 3D models at a steady heat source temperature of T_h = 450 K. (a) Output performance predicted by the 3D model with impedance matching boundary. (b) Output performance predicted by the 3D model with current input boundary.

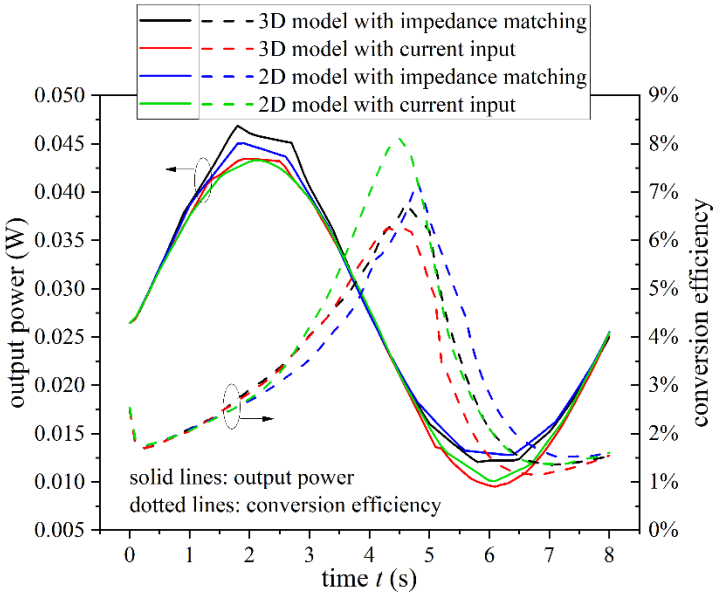

Fig. 8. Comparison of transient output power and conversion efficiency of the TEG unit predicted by four transient numerical models.

Under the conditions of optimal load resistance (R_L = 0.31 Ω) and optimal current input (I_L = 0.92 A), the transient output performances of the TEG unit predicted by four transient numerical models are obtained and compared. Fig. 8 shows the comparison of transient output power and conversion efficiency. Here, the sine wave transient heat source temperature in Fig. 3(e) is loaded on the hot side of the TEG unit. Under the same dimension, the output power predicted by the model using current input boundary is lower than that predicted by the model using impedance matching boundary. The reason for this is that the thermal inertia is underestimated in the model with current input boundary, and the output power curve is basically consistent with the transient heat source temperature curve. When the current flows through the TEG unit, the output response occurs immediately without the hysteresis of heat transfer. However, for the model with impedance matching boundary, the electricity is generated by temperature difference, and the response hysteresis of heat transfer is fully considered. Under the same boundary conditions, the fluctuation amplitude of the output power predicted by 2D models is smaller than that predicted by 3D models, especially for the model using impedance matching boundary, which is caused by the lower thermal inertia in the 2D geometry. Compared with the 3D model with impedance matching boundary, the average output power errors of 3D model with current input boundary, 2D model with impedance matching boundary, and 2D model with current input boundary are 6.11%, 2.50%, and 4.83%, respectively. In terms of transient conversion efficiency, the models with current input boundary predict more unreasonable results than the models with impedance matching boundary, because the current input boundary leads to external energy input.

Accordingly, to ensure the accuracy of transient output performance, the 3D transient thermal-electric numerical model with impedance matching boundary was used to predict the dynamic response characteristics of the TEG module in the following sections.

5. Results and discussion

5.1 Physical field distribution characteristics of the thermoelectric generator module

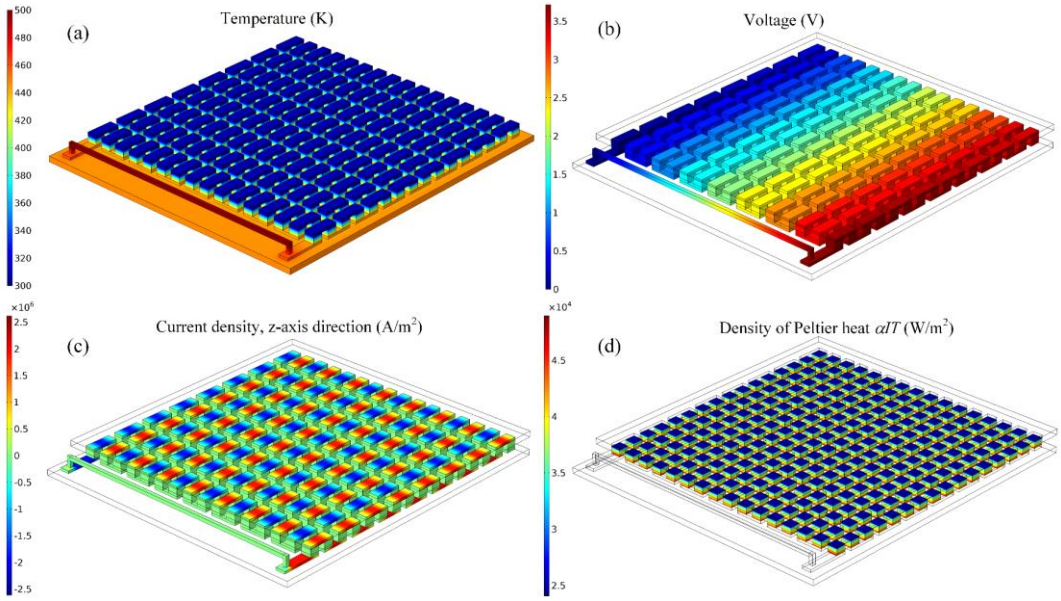

Fig. 9. Physical field distribution characteristics of the thermoelectric generator module under steady-state heat source input temperature. (a) Temperature distributions, (b) Voltage distributions, (c) Current density distributions, (d) Distributions of the Peltier heat density.

Fig. 9 shows the physical field distributions of the TEG module under steady-state heat source input temperature. Here, the load resistance is set to be equal to 4 Ω. Fig. 9(a) exhibits that the temperature drop from the hot side to the cold side of thermoelectric elements is roughly 138.25 K, which is dominant in the whole temperature difference from the heat source input temperature of 450 K to the cooling source temperature of 300 K. The low thermal conductivity of thermoelectric elements accounts for this phenomenon. Moreover, the temperature of load resistance is apparently higher than other components, caused by the Joule heat. Fig. 9(b) shows the voltage distributions of the TEG module. Driven by the temperature difference, the holes in p-type thermoelectric elements and the electrons in n-type thermoelectric elements move from the hot end to the cold end, thus generating Seebeck voltage. Thermoelectric elements are connected in series with copper electrodes to generate enough power for recycling. The output voltage shown in the figure is 3.72 V, and the output power is

3.45 W through a simple calculation. Given the high electric conductivity and low cross-sectional area, the absolute value of the current density of copper electrodes is the highest, as shown in Fig. 9(c). The opposite current density of two adjacent rows of copper electrodes is caused by the opposite flow direction of electric current. Fig. 9(d) shows the distributions of αIT along thermoelectric elements. At the junction of the hot and the cold ends, it represents the hot and the cold side Peltier heats, respectively. Given the difference in temperature, the hot side Peltier heat is higher than the cold side Peltier heat.

5.2 Determination of the maximum power point through steady-state analysis

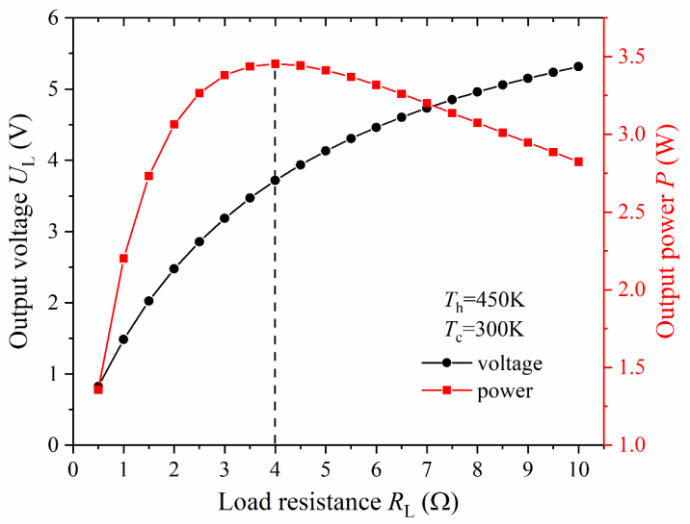

Fig. 10. Steady-state output performance of the thermoelectric generator module with different load resistances.

In practical application, the TEG module is connected with the energy recovery circuit to recycle the generated electricity. In the numerical simulation, it can be regarded that the TEG module is connected to the load resistance, and its output performance is affected by the load resistance. Before transient performance analysis, a steady-state performance investigation should be conducted to determine the optimal working point. Fig. 10 shows the steady-state output voltage and output power of the TEG module with different load resistances. When the load resistance increases, the output voltage also increases. Given that the load resistance is connected in series with the TEG module, the higher the load resistance, the higher the output voltage. When the load resistance is slightly higher than the internal resistance of the TEG module, the output power reaches the highest value, which is roughly 4 Ω. Therefore, the optimal working point of R_L = 4 Ω is selected to study the dynamic response characteristics of the TEG module under transient temperature excitations.

5.3 Dynamic output power of the thermoelectric generator module under transient temperature

excitations

The transient temperature excitation can be classified into two kinds: One is the transient temperature change between two states, that is, the heat source input temperature changes from one state to another, and then remains unchanged, for example, when the TEG module is in the start-up or shutdown stages; Another one is the periodic temperature excitation, that is, the heat source input temperature changes in a periodic trend. The cases of step increase, step decrease, linear increase, and linear decrease belong to the transient temperature change between two states, whereas the cases of the sine and triangular waves belong to the periodic temperature excitation. In this study, the dynamic response characteristics of both are studied.

5.3.1 Dynamic output power and hot side temperature of thermoelectric elements under transient temperature change

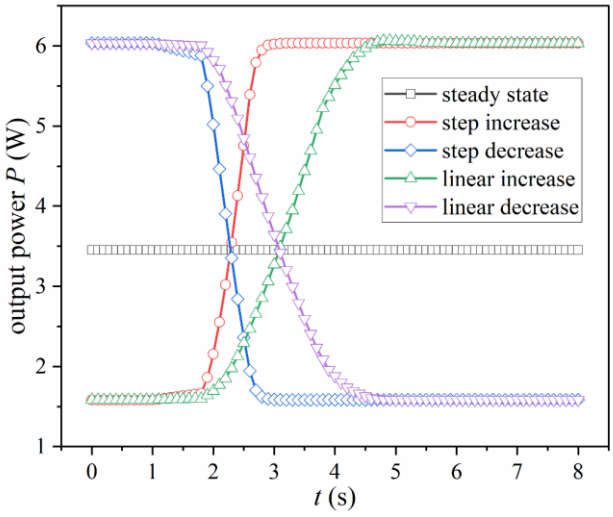

Fig. 11. Dynamic output power at the steady, step increase, step decrease, linear increase, and linear decrease states.

Fig. 11 shows the dynamic output power at the steady, step increase, step decrease, linear increase, and linear decrease states. When the heat source input temperature is step increased or step decreased, the output power represents a linear increase or linear decrease, which is caused by the continuity of internal energy. Although the temperature applied to the hot side surface of the TEG module can change rapidly between two different temperatures, the internal energy of the TEG module will respond at a slower speed and is continuous. The figure reveals that whether the heat source input temperature changes step or linearly, there is a time delay in the output power. The time delay of step increase and step decrease is around 0.9 s, whereas that of linear increase and linear decrease is around 0.6 s. Here, when the difference between the output voltage at a certain time and the output voltage at

$t \geq 6$ s is within 0.01 V, the response is considered to be finished. Seemingly, the time delay is related to the rate of temperature change. In addition, the steady-state output power is 3.45 W at T_h = 450 K, which is lower than the average output power of 3.81 W at T_h = 400 K (P = 1.58 W) and T_h = 500 K (P = 6.04 W), because the output power is not linear with the temperature difference.

To further analyse the response hysteresis phenomenon in Fig. 11, the corresponding thermal analysis is given. Fig. 12 shows the dynamic hot-side temperature of thermoelectric elements (T_{h_te}) at the step increase and linear increase states. Given the thermal resistance of the ceramic plate, the hot side temperature of thermoelectric elements (T_{h_te}) is slightly lower the heat source input temperature (T_h). In addition, the changing trend of the temperature at the hot end of the thermoelectric elements (T_{h_te}) is identical to that of the output power, which means that the time delay of the response of output power is not caused by the thermoelectric effects, but by the heat transfer. In essence, the electric response is much faster than the thermal response. For the case of step increase, the heat source input temperature begins to increase at t = 2 s, however, the corresponding hot side temperature response time is earlier than t = 2 s. The reason for this is that the heat source input temperature has undergone smoothing processing through a continuous function in COMSOL, and it is more in line with the actual situation. The corresponding change of output power between t = 1 s and t = 2 s in Fig. 11 can be explained by this phenomenon.

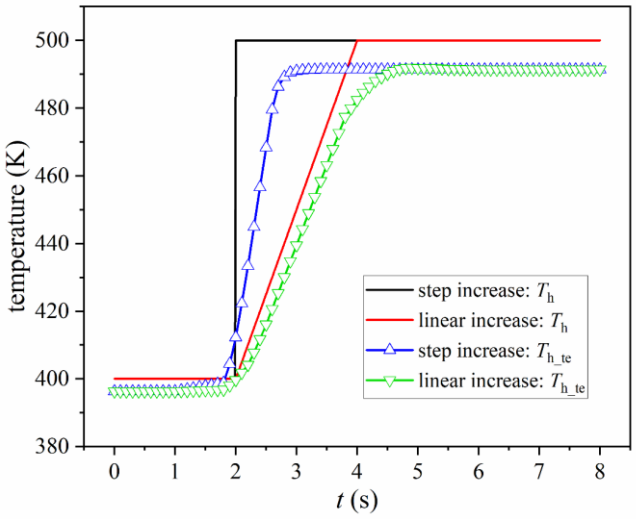

Fig. 12. Dynamic hot-side temperature of thermoelectric elements at the step increase and linear increase states.

5.3.2 Dynamic output power and hot side temperature of thermoelectric elements under periodic temperature excitation

In some practical applications, the heat source input temperature is periodic, for example, in the field of automobile exhaust waste heat recovery, the input temperature provided by exhaust gas changes

periodically when the vehicle works under driving cycles. Fig. 13 shows the dynamic output power at the steady, sine wave, and triangular wave states. The cycle period of the sine and triangle waves is 8 s. Fundamentally, there also exists a time delay in the response of output power. The time delay of the sine and the triangular waves is roughly 0.1 s, which is lower than those of step and linear temperature excitations. The rate of temperature change of the sine and the triangular waves is 25 K/s, whereas those of step and linear temperature excitations are ∞ K/s and 50 K/s, respectively. Ultimately, the time delay increases when the temperature rate increases.

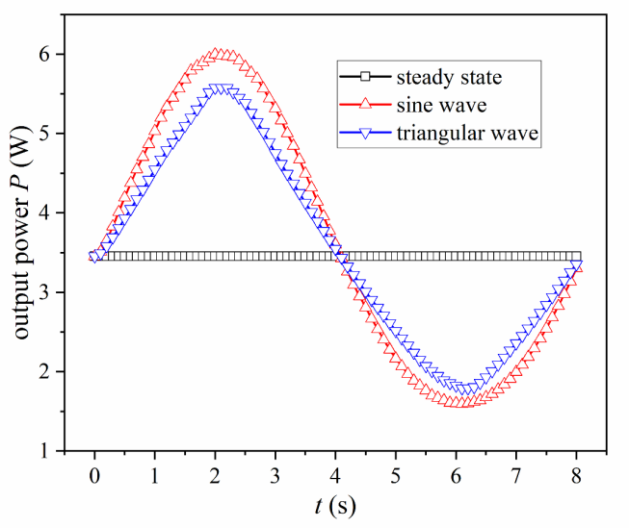

Fig. 13. Dynamic output power at the steady, sine wave, and triangular wave states.

In addition, the maximum output power of triangular wave temperature excitation is lower than that of sine wave temperature excitation. The reason for this may be that the temperature change in the case of the sine wave is smoother than that of the triangular wave. In the case of the triangular wave, when $t < 2$ s, the temperature of the TEG module rises steadily. Given the influence of time delay, when $t = 2$ s, the temperature still does not rise to the highest point. However, when $t > 2$ s, the TEG module changes from heating to cooling, so the maximum temperature can not be reached. Different from the triangular wave, for the sine wave, the rate of temperature change near $t = 2$ s is much smaller than other times, so the time delay can be ignored, and the temperature of the TEG module can reach the maximum value. The average output power of the sine wave and triangle wave is 3.62 W and 3.55 W respectively, which are 4.93% and 2.82% higher than the steady-state output power, respectively. Ultimately, the periodic heat source can amplify the output power.

Similarly, the response hysteresis of output power in Fig. 13 is mainly caused by the thermal inertia during the heat transfer process. The dynamic hot-side temperature of thermoelectric elements (T_{h_te}) under the sine wave and triangular wave temperature excitations is shown in Fig. 14. There exists a

time delay of thermal response, and the time delay is lower than those of step and linear temperature excitations. Given the continuity of heat transfer and the smoothing processing of input temperature, for the triangular wave temperature excitation, the change of hot side temperature (T_{h_te}) is smoother than the change of heat source input temperature (T_h) when the time is close to t = 2 s and t = 6 s. The highest hot-side temperature of the triangular wave is lower than that of the sine wave at t = 2 s, whereas the lowest hot side temperature is higher than that of the sine wave at t = 6 s, which can be explained by the above reasons.

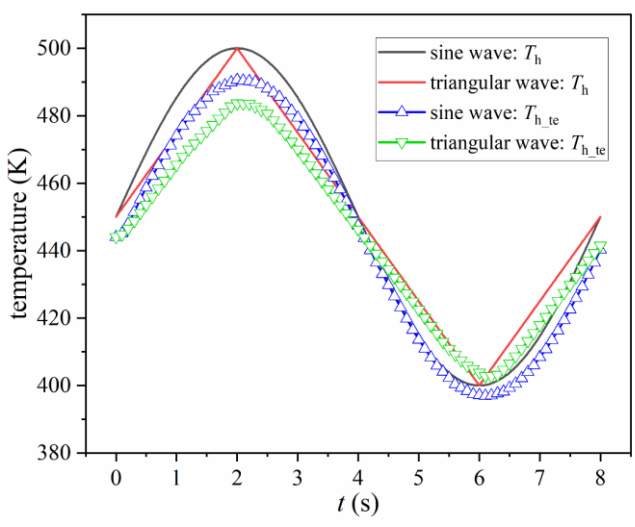

Fig. 14. Dynamic hot-side temperature of thermoelectric elements at the sine wave and triangular wave states.

5.4 Dynamic conversion efficiency of the thermoelectric generator module under transient temperature excitations

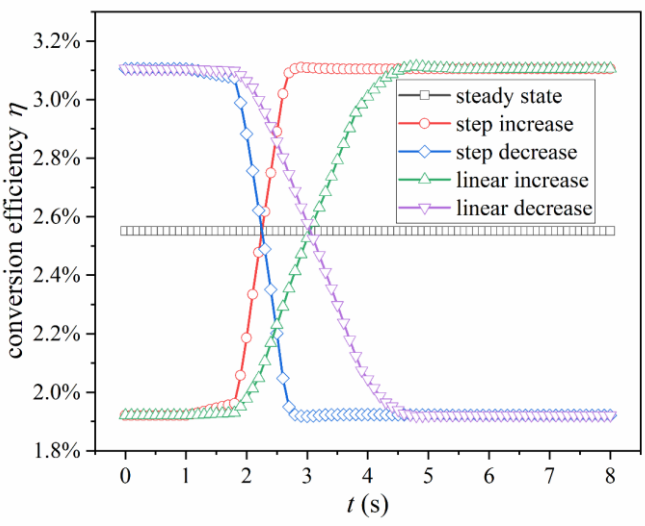

Fig. 15. Dynamic conversion efficiency at the steady, step increase, step decrease, linear increase, and linear decrease states.

Besides the output power, the conversion efficiency is also an important feature to characterise the output performance of TEG modules. Fig. 15 shows the dynamic conversion efficiency at the steady, step increase, step decrease, linear increase, and linear decrease states. When the hot side temperature increases, the TEG module produces higher output power and converts more absorbed heat into electricity. The changing trend of conversion efficiency is consistent with that of the output power. The only difference is that the steady-state conversion efficiency at T_h = 450 K is 2.55%, which is almost equal to the mean conversion efficiency (2.51%) of T_h = 400 K and T_h = 500 K. The reason for this is that the steady-state heat absorption at T_h = 450 K is 135.37 W, whereas those of T_h = 400 K and T_h = 500 K are 82.37 W and 194.34 W, respectively. In addition, the conversion efficiency exhibits the same time delay as the output power, because the conversion efficiency is proportional to the output power.

The dynamic conversion efficiency at the steady, sine wave, and triangular wave state is shown in Fig. 16. The average conversion efficiency of the TEG module under sine wave temperature excitation is 2.54%, which is the same as that under triangular wave temperature excitation, and both are almost equal to the steady-state conversion efficiency of 2.55%. Although the periodic temperature excitation can amplify the output power, it has barely any effect on conversion efficiency. Combined with the above analysis work, thus, the conversion efficiency has the same response characteristics as the output power, such as the same time delay, when the heat source input temperature changes. The output power under transient temperature excitation may be higher than that under steady-state temperature excitation, which depends on the type of transient temperature excitation. However, the conversion efficiency under transient temperature excitation is equal to that under steady-state temperature excitation.

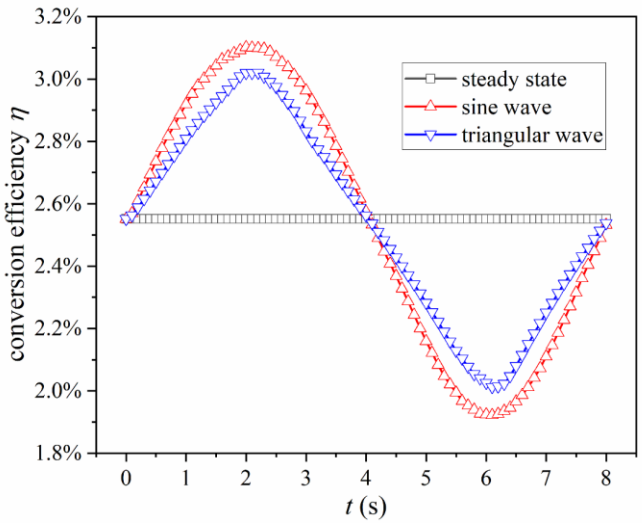

Fig. 16. Dynamic conversion efficiency at the steady, sine wave, and triangular wave states.

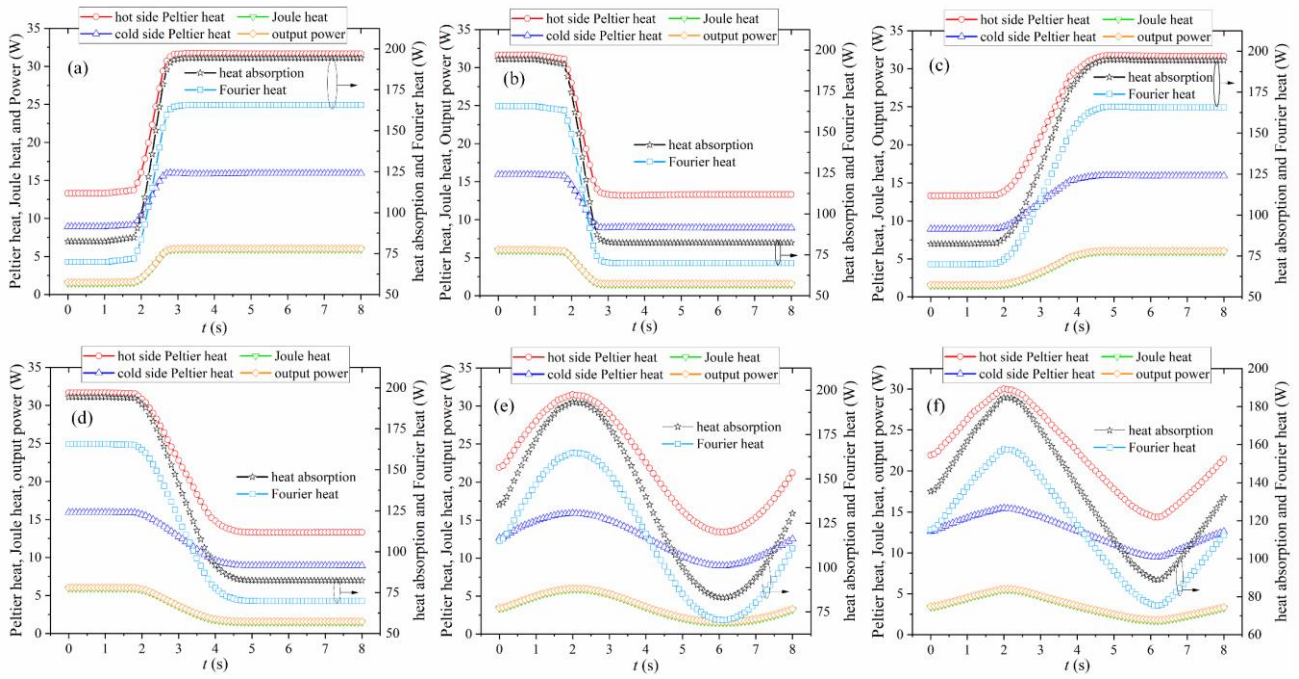

Fig. 17. Dynamic Fourier heat, Peltier heat, Joule heat, and output power under transient temperature excitations. (a) Step increase, (b) Step decrease, (c) Linear increase, (d) Linear decrease, (e) Sine wave, (f) Triangular wave.

To further study the influence of transient temperature excitation on the dynamic response characteristics of the TEG module, the thermal responses of thermoelectric elements produced by different physical effects are obtained, including heat absorption, Fourier heat, Peltier heat, Joule heat, and output power, as shown in Fig. 17. The higher the temperature, the greater the difference amongst different heat temperatures. The energy of heat absorption is the highest, followed by Fourier heat, hot side Peltier heat, cold side Peltier heat, output power, and Joule heat. Here, the heat absorption is equal to Fourier heat plus hot side Peltier heat and minus one half of the Joule heat, where Fourier heat accounts for the main part of heat absorption, which means that the conversion efficiency can be improved by reducing the thermal conductivity of thermoelectric elements. Under the transient temperature excitation, the cold side Peltier heat, Joule heat, and output power keep the same changing trend, and the changing trend is gentler than that of hot side Peltier heat. The reason for this is that the hot side Peltier heat is directly related to the primary response variable of hot side temperature, whereas the cold side Peltier heat, Joule heat, and output power are related to the secondary response variables of the cold side temperature and electric current. When the input temperature changes, the hot side temperature changes first, and then through the processes of heat transfer and thermoelectric effect, the cold side temperature and electric current respond accordingly. The output power is slightly higher

than Joule heat, because of the parasitic internal resistance in the thermoelectric elements, and the output power is equal to the sum of the two Joule heat. More details about the parasitic internal resistance can be found in Ref. [14].

6. Conclusions

In practical application, the hot side working temperature of thermoelectric generator modules provided by the heat source is time-dependent, and the steady-state analysis can not reveal the real dynamic performance. Thus, a 3D transient numerical model of the thermoelectric generator is established to study the dynamic response characteristics of a given thermoelectric generator module under transient temperature excitations. The model takes into account the heat-electric multiphysics coupling effects, the temperature dependence of thermoelectric materials, and the impedance matching characteristics, which is a comprehensive theoretical model close to the real situation. The proposed model is also compared with other transient numerical models, including a 3D model with current input boundary, a 2D model with impedance matching boundary, and a 2D model with current input boundary. Some useful results are obtained. In this work, six typical transient temperature excitations, including step increase, step decrease, linear increase, linear decrease, sine wave, and triangular wave, are used as the hot side temperature boundary conditions to analyse the dynamic output power and conversion efficiency of the thermoelectric generator module. Moreover, the dynamic output performance is compared with the steady-state output performance, and the model is verified by comparing the output voltage and output power between the numerical results and the experimental results under steady-state conditions. The main conclusions are as follows:

(1) The 3D transient numerical model takes into account the conditions in the real working environment, and can predict the dynamic output performance of thermoelectric generator modules under any transient temperature excitation. Combined with the transient modelling of heat source, the model can be further extended from the thermoelectric generator module to the whole thermoelectric generator system.

(2) When the input current is in a reasonable range, there is no difference between the model with impedance matching boundary and the model with current input boundary in the prediction of steady-state output performance, but the dynamic response characteristics predicted by the two models are quite different. To ensure the accuracy of transient output performance, a 3D transient numerical model with impedance matching boundary should be adopted, and the model should be extended from 2D to 3D.

(3) The maximum deviation of steady-state output power between numerical results and experimental data is 1.56%, which shows that the model can accurately predict the output performance under steady-state conditions. The transient experimental verification will be carried out in future work. Before the transient numerical simulations, the examinations of optimal working point and time step are conducted, and the load resistance of R_L = 4 Ω and the time step of 0.1 s are used to conduct the transient numerical simulations.

(4) When the heat source temperature changes rapidly, the corresponding output power, conversion efficiency, and other thermal responses will show a more stable change. A time delay of output responses transpires under the transient temperature excitation, and the time delay increases when the temperature rate increases. The time delay of step, linear, and sine or triangular wave temperature excitations is 0.9 s, 0.6 s, and 0.1 s, respectively.

(5) The dynamic response characteristic of the output power is synchronous with that of the conversion efficiency. The periodic temperature excitation may amplify the output power, but it hardly affects the conversion efficiency. The average output power of the sine and triangle waves is 4.93% and 2.82% respectively higher than the steady-state output power, however, the average conversion efficiency of both is almost identical to the steady-state conversion efficiency.

Acknowledgments

The authors are grateful for the financial support from the Postgraduate Research & Practice Innovation Program of Jiangsu Province (KYCX20_3012), National Natural Science Foundation of China (51977100), as well as EU ThermaSMART project under Grant No. H2020-MSCA-RISE (778104)-Smart thermal management of high power microprocessors using phase-change (ThermaSMART).

References

[1] Luo D, Wang R, Yu W, Sun Z, Meng X. Modelling and simulation study of a converging thermoelectric generator for engine waste heat recovery. Appl Therm Eng 2019;153:837-47.

[2] Champier D. Thermoelectric generators: A review of applications. Energy Convers Manage 2017;140:167-81.

[3] LaLonde AD, Pei Y, Wang H, Jeffrey Snyder G. Lead telluride alloy thermoelectrics. Mater Today 2011;14:526-32.

[4] Luo D, Wang R, Yu W, Zhou W. A numerical study on the performance of a converging

thermoelectric generator system used for waste heat recovery. Appl Energy 2020;270:115181.

[5] Ge M, Li Z, Wang Y, Zhao Y, Zhu Y, Wang S, et al. Experimental study on thermoelectric power generation based on cryogenic liquid cold energy. Energy. 2021;220:119746.

[6] Kim CS, Lee GS, Choi H, Kim YJ, Yang HM, Lim SH, et al. Structural design of a flexible thermoelectric power generator for wearable applications. Appl Energy 2018;214:131-8.

[7] Li G, Zheng Y, Hu J, Guo W. Experiments and a simplified theoretical model for a water-cooled, stove-powered thermoelectric generator. Energy. 2019;185:437-48.

[8] Liu K, Tang X, Liu Y, Xu Z, Yuan Z, Li J, et al. Preparation and optimization of miniaturized radioisotope thermoelectric generator based on concentric filament architecture. J Power Sources 2018;407:14-22.

[9] Wang Y, Li S, Xie X, Deng Y, Liu X, Su C. Performance evaluation of an automotive thermoelectric generator with inserted fins or dimpled-surface hot heat exchanger. Appl Energy 2018;218:391-401.

[10] Nozariasbmarz A, Suarez F, Dycus JH, Cabral MJ, LeBeau JM, Öztürk MC, et al. Thermoelectric generators for wearable body heat harvesting: Material and device concurrent optimization. Nano Energy. 2020;67:104265.

[11] Montecucco A, Siviter J, Knox AR. Combined heat and power system for stoves with thermoelectric generators. Appl Energy 2017;185:1336-42.

[12] Yilbas BS, Sahin AZ. Thermoelectric device and optimum external load parameter and slenderness ratio. Energy. 2010;35:5380-4.

[13] Luo D, Wang R, Yu W, Zhou W. Parametric study of a thermoelectric module used for both power generation and cooling. Renewable Energy 2020;154:542-52.

[14] Luo D, Wang R, Yu W, Zhou W. Parametric study of asymmetric thermoelectric devices for power generation. Int J Energy Res 2020;44:6950-63.

[15] Meng J-H, Zhang X-X, Wang X-D. Characteristics analysis and parametric study of a thermoelectric generator by considering variable material properties and heat losses. Int J Heat Mass Transfer 2015;80:227-35.

[16] Luo D, Wang R, Yu W. Comparison and parametric study of two theoretical modeling approaches based on an air-to-water thermoelectric generator system. J Power Sources 2019;439:227069.

[17] Luo D, Wang R, Yu W, Zhou W. Performance optimization of a converging thermoelectric generator system via multiphysics simulations. Energy. 2020;204:117974.

[18] Luo D, Wang R, Yu W, Zhou W. A novel optimization method for thermoelectric module used

in waste heat recovery. Energy Convers Manage 2020;209:112645.

[19] Khajepour A, Rahmani F. An approach to design a 90Sr radioisotope thermoelectric generator using analytical and Monte Carlo methods with ANSYS, COMSOL, and MCNP. Appl Radiat Isot 2017;119:51-9.

[20] Ma T, Lu X, Pandit J, Ekkad SV, Huxtable ST, Deshpande S, et al. Numerical study on thermoelectric–hydraulic performance of a thermoelectric power generator with a plate-fin heat exchanger with longitudinal vortex generators. Appl Energy 2017;185:1343-54.

[21] Chen M, Rosendahl LA, Condra T. A three-dimensional numerical model of thermoelectric generators in fluid power systems. Int J Heat Mass Transfer 2011;54:345-55.

[22] Luo D, Wang R, Yu W, Zhou W. Performance evaluation of a novel thermoelectric module with BiSbTeSe-based material. Appl Energy 2019;238:1299-311.

[23] Gou X, Yang S, Xiao H, Ou Q. A dynamic model for thermoelectric generator applied in waste heat recovery. Energy. 2013;52:201-9.

[24] Lan S, Yang Z, Chen R, Stobart R. A dynamic model for thermoelectric generator applied to vehicle waste heat recovery. Appl Energy 2018;210:327-38.

[25] Chen M, Rosendahl LA, Condra TJ, Pedersen JK. Numerical Modeling of Thermoelectric Generators With Varing Material Properties in a Circuit Simulator. IEEE Trans Energy Convers 2009;24:112-24.

[26] Fisac M, Villasevil FX, López AM. Design of a thermoelectric generator with fast transient response. Renewable Energy 2015;81:658-63.

[27] Meng J-H, Wu H-C, Gao D-Y, Kai Z, Lu G, Yan W-M. A novel super-cooling enhancement method for a two-stage thermoelectric cooler using integrated triangular-square current pulses. Energy. 2021;217:119360.

[28] Meng J-H, Wu H-C, Wang L, Lu G, Zhang K, Yan W-M. Thermal management of a flexible controlled thermoelectric energy conversion-utilization system using a multi-objective optimization. Appl Therm Eng 2020;179:115721.

[29] Yan Y, Malen JA. Periodic heating amplifies the efficiency of thermoelectric energy conversion. Energy Environ Sci 2013;6:1267-73.

[30] Meng J-H, Zhang X-X, Wang X-D. Dynamic response characteristics of thermoelectric generator predicted by a three-dimensional heat-electricity coupled model. J Power Sources 2014;245:262-9.

[31] Jia X-D, Wang Y-J, Gao Y-W. Numerical simulation of thermoelectric performance of linear-

shaped thermoelectric generators under transient heat supply. Energy. 2017;130:276-85.

[32] Liao M, He Z, Jiang C, Fan Xa, Li Y, Qi F. A three-dimensional model for thermoelectric generator and the influence of Peltier effect on the performance and heat transfer. Appl Therm Eng 2018;133:493-500.